EPJ Web of Conferences **3**, 06001 (2010)
DOI:10.1051/epjconf/20100306001

Electromagnetic interactions in Halo Effective Field Theory

R. Higa[1,2,a]

[1] Helmholtz-Institut für Strahlen- und Kernphysik, Universität Bonn, Nußallee 14-16, 53115 Bonn, Germany
[2] Kernfysisch Versneller Instituut, Rijksuniversiteit Groningen, Zernikelaan 25, 9747 AA Groningen, The Netherlands

Abstract. After a brief discussion of effective field theory applied to nuclear clusters, I concentrate on the inclusion of two particular aspects, namely, narrow resonances and electromagnetic interactions. As examples of applications, I present the details of our studies on alpha-alpha and proton-alpha scattering.

1 Introduction

Two-particle scattering at low enough energies are insensitive to the details of the interparticle interaction, provided that the latter has a limited range of action. The intuitive argument behind this general property is that momenta whose wavelengths are much larger than the interaction range cannot resolve its finer details. The elastic amplitude incorporates unitarity constraints and an universal low-energy expansion, *a.k.a.* the effective range expansion (ERE), whose coefficients encode the low-energy behavior of the forces for a particular system. This simple observation, made by Bethe and others [1] more than fifty years ago, became a benchmark for theorists trying to model the dynamics of the interaction.

The same line of reasoning is shared by effective field theories (EFT), where only the relevant low-energy degrees of freedom are explicitly taken into account. Modes that are active only at high energies are "frozen" into the low-energy constants. In the particular case of EFT with short-range interactions, the two-body scattering amplitude is equivalent to a low-energy expansion of the ERE amplitude [2]. However, the EFT approach has extra features over the effective range theory. First, the systematic expansion of the amplitude allows for a reliable and unbiased estimate of the theoretical uncertainties. Second, symmetries of the problem or the way they are broken can be implemented in a straightforward way (for instance, electromagnetic and weak currents, isospin, parity). And third, the ability to extend the formalism to systems with more than two particles.

One example of the second feature illustrates a difference between the EFT and ERE approaches. In the process $np \to d\gamma$, the $M1_v$ transition contains at NLO a four-nucleon-photon operator that cannot be generated by the ERE approach [3]. The associated coupling can be fixed from cold neutron capture rate at incident neutron speed of 2200 m/s. Rupak improved the calculation of $M1_v$ and $E1_v$ transitions to N^2LO and N^4LO, respectively, lowering the theoretical uncertainty in the $np \to d\gamma$ reaction to about 1% for center-of-mass energies up to 1 MeV [4].

When extended to three or more particles with large scattering length(s), EFT provides new insights and explains certain universal properties that are independent of the interaction details. For instance, the related Thomas and Efimov effects [5] are intimately connected to the behavior of the leading three-body counterterm under variations of the momentum cutoff in the dynamical equations. Such counterterm is necessary to properly renormalize the theory, as well as to guarantee a unique solution in the limit when the cutoff is taken to infinity [6,7]. It exhibits a limit cycle behavior, that is, a log-periodic dependence with the cutoff, that explains the geometrically-separated bound states in the Efimov spectrum. For nuclear systems with three and four nucleons, the theory provides a convincing explanation to certain correlations, like the almost linear dependence of the spin-doublet neutron-deuteron scattering length with the triton binding energy [8,9] or similar dependence of the latter with the alpha particle binding energy [10], known respectively as the Phillips and Tjon lines.

Due to the universal character, effective field theories with short-range interactions have been successfully applied to distinct areas of physics —atomic, particle, and few hadron systems. For a more complete overview, see Refs. [6,11]. Here I will concentrate on applications to nuclei that behave as systems of loosely bound clusters, which also include the nowadays popular halo nuclei. In Section 2 the general features of the so-called halo/cluster EFT are presented in certain detail, with emphasis on aspects quite often faced when dealing with nuclear clusters. Sections 3 and 4 present applications of halo/cluster EFT to alpha-alpha ($\alpha\alpha$) and proton-alpha ($p\alpha$) scattering, and in Section 5 are the concluding remarks.

2 EFT for nuclear clusters

The relevant degrees of freedom in halo/cluster EFT are the structureless, weakly bound objects represented by re-

[a] e-mail: R.Higa@rug.nl

spective field operators. In the case of halo nuclei, these are the core nucleus and the valence nucleons. Effects like nucleon excitations inside the core, pion or nucleon exchanges, take place at energies well above the binding energy that holds the clusters together. The former has an associated momentum scale M_{hi} of the order of the inverse of the interaction range, while in the latter case the momentum scale $M_{lo} \ll M_{hi}$ is inversely proportional to the size of the halo system. As explained in the following, this separation of scales is, from the EFT point of view, the outcome of a fine-tune in the coupling constants, similar to the one responsible for generating a shallow bound state in the spin-triplet nucleon-nucleon channel. In fact, due to its large extension compared to the typical range of the proton-neutron interaction, the deuteron can be seen as the simplest halo nucleus, with a loosely bound neutron surrounding a proton core.

In order to understand the formalism, let us consider a system of identical bosons, with mass m_α, represented by a field ϕ and interacting via a pairwise S-wave short-range force. The most general Lagrangian respecting the relevant symmetries of the system (parity, total angular momentum, approximate isospin and non-relativistic Galilean invariance) is given by

$$\mathcal{L} = \phi^\dagger \left[i\partial_0 + \frac{\nabla^2}{2m_\alpha} \right] \phi - d^\dagger \left[i\partial_0 + \frac{\nabla^2}{4m_\alpha} - \Delta \right] d + g \left[d^\dagger \phi\phi + (\phi\phi)^\dagger d \right] + \cdots , \quad (1)$$

where we introduce an auxiliary (dimeron) field d, with "residual mass" Δ, carrying the quantum numbers of two bosons in S-wave and coupling with their fields through the coupling constant g. The dots stand for higher order terms in a derivative expansion. The building blocks are the boson and dimeron propagators, the LO coupling g between the dimeron and two boson fields, and higher-order couplings that can be rewritten, via field redefinitions, as powers of the dimeron kinetic energy. The boson and dimeron propagators read

$$iS_\alpha(q_0; \mathbf{q}) = \frac{i}{q_0 - \mathbf{q}^2/2m_\alpha + i\epsilon} , \quad (2)$$

$$iD(q_0; \mathbf{q}) = -\frac{i}{q_0 - \mathbf{q}^2/4m_\alpha - \Delta + i\epsilon} , \quad (3)$$

where the precise form of the latter depends on the magnitude of each term in the denominator. The power counting specifies the amount of fine-tuning in the low-energy couplings, responsible for assigning a well-defined order to every possible Feynman diagram that contributes to the scattering amplitude. In a natural scenario, where fine-tuning is absent, the effective couplings in Eq.(1) depend only on the high-energy scale M_{hi} of the theory. That corresponds to $\Delta \sim M_{hi}^2/m_\alpha$ and $g^2 \sim M_{hi}/m_\alpha^2$. The bare dimeron propagator (3) is static at leading order (LO),

$$iD(p_0; \mathbf{p}) \simeq \frac{-i}{-\Delta + i\epsilon} \sim O(m_\alpha/M_{hi}^2) .$$

The LO tree diagram is proportional to $a_0 = m_\alpha g^2/4\pi\Delta \sim O(1/M_{hi})$, where a_0 is the boson-boson scattering length. The one-loop graph receives two additional factors from the coupling constant g, one dimeron propagator, one-loop integration measure $dq_0\, d^3q \sim k^5/m_\alpha$, and two intermediate boson propagators $S_\alpha^2 \sim (m_\alpha/k^2)^2$. The net result is a suppression of k/M_{hi} compared to the tree graph, with k the typical low-energy momentum under consideration. The next order, k^2/M_{hi}^2 smaller than the tree level, comprises two-loop contributions proportional to $(a_0 k)^2$ and one kinetic term insertion to the dimeron propagator proportional to $a_0 r_0 k^2$, where $r_0 = 4\pi/m_\alpha^2 g^2 \sim 1/M_{hi}$ is the boson-boson effective range. The amplitude then amounts to a simple Taylor expansion in powers of the expansion parameter k/M_{hi}.

However, a natural perturbative treatment is unable to account for a plethora of nuclear phenomena, where bound states and resonances are the rule rather than exceptions. That demands a certain amount of fine-tuning in the parameters of the effective Lagrangian. The physics of shallow S-wave bound states can be described by fine-tuning the parameter Δ in Eq.(1), responsible for driving the size of the scattering length a_0. Setting $\Delta \sim M_{hi} M_{lo}/m_\alpha$ leads to a large $a_0 \sim 1/M_{lo}$, with M_{lo} the new momentum scale associated to the fine-tuning. This situation is analogous to the nucleon-nucleon (NN) case [6,7]. A consequence of this new scale is that higher-loop graphs built up from the LO boson-boson-dimeron coupling g are no longer suppressed when $k \sim M_{lo}$, but contribute at the same order as the lower-loop and tree graphs. The resummation of this class of diagrams leads to a LO amplitude in the form of a truncated effective range expansion up to its first coefficient. The scattering length then becomes the only relevant scale and (for positive values) predicts the existence of a shallow bound state $E_B \approx 1/(m_\alpha a_0^2)$. The renormalization group (RG) analysis of the Schrödinger equation demonstrates that two-body systems with large scattering length consist of strongly interacting systems with an RG-flow towards a non-trivial fixed point [12], in contrast to the natural case of weakly interacting particles, where the RG flows towards a stable, trivial fixed point.

When extended to three-body systems, this EFT provides new insights on some universal features, as mentioned in the introduction. An investigation searching for these universal effects in two-neutron halos was performed in Ref. [13], where it was found the ^{20}C nuclei as possible candidate to have an Efimov-like spectrum (see also [14]). Non-universal (effective range) corrections have recently being incorporated to this study [15].

There is an additional phenomenum quite often present in nuclear clusters, namely, the existence of low-energy resonances in the continuum. One could then expect the need for extra amount of fine-tuning. This is the case for neutron-alpha ($n\alpha$) scattering [16,17], where the presence of a narrow resonance in the $P_{3/2}$ channel around $E_n \approx 1$ MeV requires adjustment of the coupling constants of the theory to enhance the $P_{3/2}$ amplitude a few orders of magnitude away from the natural assumption. Another example is the $\alpha\alpha$ system [18], which contains an S-wave resonance about 0.1 MeV above the elastic threshold. The $\alpha\alpha$ scattering amplitude can be described by the Lagrangian

(1), but assuming $\Delta \sim M_{lo}^2/m_\alpha$. This is necessary to generate an even larger $\alpha\alpha$ scattering length, $a_0 \sim M_{hi}/M_{lo}^2$. These scalings will be discussed in detail in the next section. With this power-counting the dimeron propagator is no longer static, as the kinetic and residual mass terms are now of comparable order. In momentum space it has the form of Eq.(3). The presence of the kinetic term in the dimeron propagator in practice resums effective range r_0 corrections to all orders. This resummation is necessary to reproduce a narrow resonance at low energy[18,16,17].

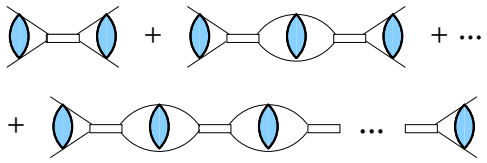

Fig. 1. Graphic representation of T_{CS}, as sum of graphs with multiple insertions of the bare dimeron propagator (double line) and the "Coulomb bubble loop". The latter contains intermediate Coulomb photons resummed to all orders (shaded ellipse).

For the case of charged bosons, electromagnetic interactions can be incorporated into Eq.(1) via the usual minimal substitution. Among them, Coulomb photons are the dominant ones at low energies [18]. Coulomb interactions were formulated in the EFT framework by Kong and Ravndal [19] for the two-proton system, and can be extended in a straightforward way to include resonances [18]. The idea relies on the two-potential formalism, where the amplitude is separated in a term that contains only the two-particle pure Coulomb scattering T_C, plus the Coulomb-modified strong amplitude T_{CS}. The latter is diagramatically illustrated by Fig. 1 (see caption) and has the form of a geometric series. Like in the proton-proton case [19], the power counting for narrow resonances demands its resummation. Up to next-to-leading order (NLO) one gets for our two-boson example, with reduced mass μ and charge Z_α,

$$T_{CS} = -\frac{2\pi}{\mu} C_\eta^2 e^{2i\sigma_0} \left[\frac{1}{-\frac{1}{a_0}+k^2\frac{r_0}{2}-2k_C H} + \frac{\mathcal{P}_0}{4} \frac{k^4}{(-\frac{1}{a_0}+k^2\frac{r_0}{2}-2k_C H)^2} \right], \quad (4)$$

where

$$k_C = \frac{\mu Z_\alpha^2 e^2}{4\pi} = \mu Z_\alpha^2 \alpha_{em} \quad (5)$$

is the inverse of the Bohr radius, and $\mathcal{P}_0$, the shape parameter. The strength of Coulomb photons is driven by the Sommerfeld parameter

$$\eta(k) = \frac{k_C}{k}, \quad (6)$$

and the Coulomb-modified strong amplitude is modulated by the Sommerfeld factor,

$$C_\eta^2 = \frac{2\pi\eta}{e^{2\pi\eta}-1}, \quad (7)$$

which quantifies the probability of finding the two bosons at the same point in space. The phase of pure Coulomb relative to free scattering, for a given partial wave L, reads

$$\sigma_L = \arg\Gamma(L+1+i\eta) = \frac{1}{2i}\ln\left[\frac{\Gamma(L+1+i\eta)}{\Gamma(L+1-i\eta)}\right]. \quad (8)$$

The last Coulomb ingredient in Eq.(4) is the function

$$H(\eta) = \psi(i\eta) + (2i\eta)^{-1} - \ln(i\eta), \quad (9)$$

and explicitly shows the complicated analytic structure of Coulomb scattering at low energies. Nevertheless, apart from the Sommerfeld factor and the S-wave Coulomb phase, one notices that the effect of dressing the strong amplitude with non-perturbative Coulomb photons amounts to, apart from a multiplicative factor in the numerator, replacing the unitarity term $-ik$ by $-2k_C H(\eta)$ in the denominator of the amplitude. Similar expression can be derived for P-wave interactions and will be presented in Section 4.

3 $\alpha\alpha$ scattering

3.1 power counting: pinning the scales down

In order to better understand the scalings of the EFT parameters in the presence of a resonance, it is helpful to provide some numbers for the relevant physical quantities. It is well-known that the $\alpha\alpha$ system is dominated by S-wave at low energies [20], having a very narrow resonance at $E_R \simeq 92$ keV and width $\Gamma_R \approx 6$ MeV. To this resonance is commonly assigned the ^{8}Be ground state. The $\alpha\alpha$ scattering length $a_0 \sim 2000$ fm is about three orders of magnitude larger than the α matter radius, suggesting the large amount of fine-tuning discussed in the last section. In contrast, the effective range $r_0 \approx 1$ fm and shape parameter $\mathcal{P}_0 \approx -1.7\text{fm}^3$ obey the expected natural scalings of $1/M_{hi}$ and $1/M_{hi}^3$, respectively. It seems therefore reasonable to start with the scalings $\Delta \sim M_{lo}^2/\mu$ and $g^2/2\pi \sim M_{hi}/\mu^2$. With the evaluation of Feynman diagrams and after the required resummation described in the previous section one finds

$$T_{CS} = -\frac{2\pi}{\mu} C_\eta^2 e^{2i\sigma_0} \left[-\frac{2\pi\Delta^{(R)}}{\mu g^2} + \frac{\pi}{\mu g^2} k^2 - 2k_C H(\eta) \right]^{-1} + \cdots \quad (10)$$

where $\Delta^{(R)}$ is the only parameter in the Lagrangian, up to NLO, that is renormalized by the Coulomb loops,

$$\Delta^{(R)} = \Delta(\kappa) + \frac{\mu g^2}{2\pi} \left\{ \frac{\kappa}{D-3} + 2k_C \left[\frac{1}{D-4} - \ln\left(\frac{\sqrt{\pi}\kappa}{2k_C}\right) - 1 + \frac{3}{2} C_E \right] \right\}, \quad (11)$$

with D the number of space-time dimensions, κ the renormalization scale parameter, and $C_E = 0.577\ldots$ the Euler-Mascheroni constant. The amplitude matches with the expansion of the ERE amplitude (4), from where one identifies the ERE parameters in terms of the EFT couplings.

One then finds $a_0 \sim M_{hi}/M_{lo}^2$. The low-energy scale $M_{lo} \sim \sqrt{m_\alpha E_R} \approx 20$ MeV is nearly seven times smaller than a high momentum scale associated to either the pion mass or the excitation energy of the alpha particle, $M_{hi} \sim m_\pi \sim \sqrt{m_\alpha E_\alpha^*} \approx 140$ MeV. Based on these numbers, one could expect convergent results for observables at laboratory energies up to 3 MeV.

The Bohr momentum k_C provides the scale of Coulomb interactions. Due to the large $\alpha\alpha$ reduced mass in its definition (5), k_C turns out to be numerically of the order of M_{hi}. One can therefore expects large and important electromagnetic contributions. Nevertheless, it is interesting to discuss the other limit $k_C \to 0$, when Coulomb is turned off. In this case one has $2k_C H(\eta) \to ik$ and the denominator of the LO amplitude reads

$$T_{\rm LO}^{-1} \propto -1/a_0 + r_0 k^2/2 - ik\,. \qquad (12)$$

For momenta $k \sim M_{lo}$ the first two terms are suppressed by M_{lo}/M_{hi} compared to the last one. Therefore, all that is left at LO is the unitary term $1/(-ik)$. In this limit, the ^{8}Be system exhibits non-relativistic conformal invariance [21] and the corresponding three-body system, ^{12}C, acquires an exact Efimov spectrum [6,8]. If it was possible to somehow shield the charges of the α particles, the above limit strongly suggests that two and three chargless α particles would probably be the best nuclear systems to observe few-body universality. The above scenario certainly changes for a physical value of k_C, due to the breaking of conformal invariance by the $1/r$ Coulomb force. Nevertheless, the fact that the ground state of ^{8}Be and the Hoyle state in ^{12}C remain very close to the threshold into α-particles suggests that this conformal picture is not far from the real case.

The breaking of scale invariance by the Coulomb interaction introduces the scale k_C in the propagation of two charged particles. As we have seen in Eq. (4), the unitarity term is modified. The balance between strong-interaction terms and Coulomb-modified propagation now depends on both the strong-interaction scale M_{lo} and k_C. While the former is $k_R = \sqrt{m_\alpha E_R} \sim 20$ MeV, the latter is $k_C = \alpha_{em} Z_\alpha^2 \mu \sim 60$ MeV, and therefore a relative strength of $k_C/k_R \sim 3$. For momenta $k \sim k_R$, we are clearly in the deep non-perturbative Coulomb region. The Sommerfeld parameter η reaches large values and the function $2k_C H(\eta)$ is very different from the usual unitarity term ik. Instead of hampering any simplification, it actually allows a low-energy expansion of the Coulomb function H. Using Stirling's series,

$$\ln\Gamma(1+z) = \frac{1}{2}\,\ln 2\pi + \left(z+\frac{1}{2}\right)\ln z - z + \frac{1}{12z} - \frac{1}{360z^3} + \cdots\,, \qquad (13)$$

and $\psi(z) \equiv (d/dz)\ln\Gamma(z)$ in Eq. (9) gives

$$H(\eta) = \frac{1}{12\eta^2} + \frac{1}{120\eta^4} + \cdots + \frac{i\pi}{e^{2\pi\eta}-1}\,. \qquad (14)$$

The unitarity term is thus replaced by $2k_C H(\eta) \sim k^2/6k_C$ at LO. This is now a factor $k/6k_C$ smaller in magnitude than the unitarity term in the absence of Coulomb, and comparable to the effective-range term coming from the dimeron kinetic term. One can grasp it automatically if one considers $3k_C \sim M_{hi}$, as it appears to be the case numerically.

3.2 resonance pole expansion

Before incorporating the simplifications on the function $H(\eta)$, one should take a careful look at the EFT amplitude up to NLO. First, an isolated remark. Since we assume that $\mathcal{P}_0$ is a parametrically small correction, one is allowed to reshuffle the perturbative series and resum $\mathcal{P}_0$ to all orders, thus recovering the ERE formula,

$$T_{CS}^{(\rm ERE)} = -\frac{2\pi}{\mu}\,\frac{C_\eta^2\, e^{2i\sigma_0}}{-1/a_0 + k^2\, r_0/2 - k^4\,\mathcal{P}_0/4 - 2k_C H}\,. \qquad (15)$$

Second, one notices that equation (4) is valid for generic momenta $k \sim M_{lo}$. However, it fails in the immediate proximity of k_R. This situation is familiar from the neutron-alpha case [17]. The power counting works for $k \sim M_{lo}$ except in the narrow region $|k - k_R| = O(M_{lo}^2/M_{hi})$ where the LO denominator approaches zero and a resummation of the NLO term, here associated with the shape parameter, is required. As one gets closer to the resonance momentum k_R, higher-order terms in the ERE are kinematically fine-tuned as well. This happens because the imaginary part of the denominator is exponentially suppressed by a factor $\exp(-2\pi\eta_R) \sim 10^{-8}$ and the real part is allowed to be arbitrarily small. Nevertheless, this kinematical fine-tuning is not a conceptual problem. From the EFT point of view, each new fine-tuning can be accommodated by reshuffling the series and redefining the pole position. Such a procedure works fine with a small number of kinematical fine-tunings, but is not practical in the $\alpha\alpha$ system. A better alternative is to perform an expansion around the resonance pole position, starting from the resummed (ERE) amplitude. The situation here is nearly identical to the NN system, where one can choose to expand the amplitude around the bound-state pole [22] rather than around zero energy.

A great simplification is achieved from the fact that the resonance lies in the deep Coulomb regime, where Eq. (14) provides an accurate representation of H up to the precision we are considering. The real terms shown in Eq. (14) then become an expansion in powers of $\sim (k/3k_C)^2 = O(k^2/M_{hi}^2)$. Given the asymptotic feature of the Stirling's series, at some point the remaining terms can no longer be expanded; at that point the remainder should be treated exactly. In lowest orders, however, we can use the successive terms shown in Eq. (14): numerically, the terms up to η^{-4} work to better than 3% for $E_{LAB} = 3$ MeV.

The expansion (14) not only simplifies a complicated function of k_C/k, but also makes the physics around the resonance more transparent. Since the "size" of the resonance, $1/k_R$, is much larger than the Bohr radius $1/k_C$, the Coulomb interaction is effectively short ranged, and the real part of H resembles the ERE expansion. In the amplitude T_{CS} the different strong and Coulomb coefficients proportional to a common power of k can be grouped

together, where one observes that they have comparable sizes. We therefore define

$$\tilde{r}_0 = r_0 - \frac{1}{3k_C}\,, \qquad \tilde{\mathcal{P}}_0 = \mathcal{P}_0 + \frac{1}{15k_C^3}\,, \tag{16}$$

and so on. Up to NLO we rewrite T_{CS} as

$$\begin{aligned} T_{CS} &= -\frac{2\pi}{\mu}\,\frac{C_\eta^2\, e^{2i\sigma_0}}{-1/a_0 + \tilde{r}_0 k^2/2 - \tilde{\mathcal{P}}_0 k^4/4 - ikC_\eta^2} \\ &= -\frac{2\pi}{\mu}\,\frac{C_\eta^2\, e^{2i\sigma_0}}{\tilde{r}_0(k^2-k_R^2)/2 - \tilde{\mathcal{P}}_0(k^4-k_R^4)/4 - ikC_\eta^2} \\ &= -\frac{2\pi}{\mu}\,C_\eta^2\, e^{2i\sigma_0}\Bigg[\underbrace{\frac{1}{\tilde{r}_0(k^2-k_R^2)/2 - ikC_\eta^2}}_{\text{LO term}} \\ &\quad + \underbrace{\frac{\tilde{\mathcal{P}}_0}{4}\,\frac{(k^4-k_R^4)}{(\tilde{r}_0(k^2-k_R^2)/2 - ikC_\eta^2)^2} + \ldots}_{\text{NLO correction}}\Bigg], \end{aligned} \tag{17}$$

where

$$k_R^2 = \frac{2}{a_0\tilde{r}_0}\Bigg(\underbrace{1}_{\text{LO term}} - \underbrace{\frac{\tilde{\mathcal{P}}_0}{a_0\tilde{r}_0^2}}_{\text{NLO correction}} + \ldots\Bigg). \tag{18}$$

From this expression one sees directly that $k_R \sim M_{lo}$, with corrections of $O(M_{lo}^2/M_{hi}^2)$. Note that we keep the exact form of the imaginary term in Eq. (17): even though it is negligible at $k \sim k_R$, it has an important exponential dependence on the energy responsible for keeping the phase shifts real in the elastic regime.

When $a_0 < 0$ and $r_0 < 1/3k_C$, we have $k_R^2 > 0$ and the two poles of Eq. (17) are located in the lower half of the complex-momentum plane very near the real axis, as expected for a narrow resonance. The amplitude T_{CS} can be written in terms of the resonance energy $E_R = k_R^2/2\mu$ and the resonance width $\Gamma(E)$ as[1]

$$T_{CS} = \frac{2\pi e^{2i\sigma_0}}{\mu\sqrt{2\mu E}}\,\frac{\Gamma(E)/2}{E - E_R + i\Gamma(E)/2}\,. \tag{19}$$

One finds that

$$\begin{aligned} \Gamma(E) = \Gamma(E_R)\frac{e^{2\pi k_C/k_R}-1}{e^{2\pi k_C/k}-1}\Bigg[&\underbrace{1}_{\text{LO term}} \\ &\underbrace{-\frac{\mu^2\tilde{\mathcal{P}}_0}{2\pi k_C}\left(e^{2\pi k_C/k_R}-1\right)\frac{\Gamma(E_R)}{2}(E-E_R) + \ldots}_{\text{NLO correction}}\Bigg], \end{aligned} \tag{20}$$

where

$$\Gamma(E_R) = -\frac{4\pi k_C}{\mu\tilde{r}_0}\,\frac{1}{e^{2\pi k_C/k_R}-1}\Bigg(\underbrace{1}_{\text{LO term}} + \underbrace{\frac{\tilde{\mathcal{P}}_0 k_R^2}{\tilde{r}_0}}_{\text{NLO correction}} + \ldots\Bigg). \tag{21}$$

[1] See also Ref.[23].

The width is very small because of the large value of $2\pi k_C/k_R$ in the exponential.

In the form of Eqs. (19) and (20) we can keep E_R and $\Gamma(E_R)$ fixed at each order in the expansion. Note that these equations do not change to this order if one makes a different choice —*e.g.*, $(k^2 - k_R^2)^2$ instead of $k^4 - k_R^4$— for the form of the $\tilde{\mathcal{P}}_0$ term in Eq. (17). The behavior of the phase shift around E_R is guaranteed to be of a resonant type, as it automatically satisfies the constraints

$$\delta_0^c(E_R) = \frac{\pi}{2} \quad \text{(resonance energy)}\,, \tag{22}$$

and

$$\left(\frac{d\delta_0^c(E)}{dE}\right)_{E_R} = \frac{2}{\Gamma(E_R)} \quad \text{(resonance width)}\,. \tag{23}$$

3.3 confronting the data

Unfortunately $\alpha\alpha$ scattering data at low energies are not abundant. Nevertheless, all the existing measurements at E_{LAB} up to 5 MeV show that it is dominated by the S wave, thanks to the presence of the $(J^\pi, I) = (0^+, 0)$ resonance immediately above threshold. Early determinations of the 0^+ resonance energy were performed in reactions like $^{11}\mathrm{B} + p \to 2\alpha + \alpha$ (see [20] and references therein). Later measurements of the scattering of ^{4}He atoms on $^4\mathrm{He}^+$ ions, especially projected to scan the resonance energy region and supplemented with a detailed analysis [24,25] improved the determination of the resonance energy and width to their currently accepted values, $E_{LAB}^R = 184.15 \pm 0.07$ keV and $\Gamma_{LAB}^R = 11.14 \pm 0.50$ eV [25]. The resonance CM momentum is thus $k_R = \sqrt{\mu E_{LAB}^R} \approx 18.5$ MeV.

The obvious way to extract the ERE parameters from the S-wave phase shift is to fit (the cotangent of) the latter to the ERE formula. However, fits to $\alpha\alpha$ scattering data alone are not able to constrain well those parameters and, apart from the large uncertainties, don't seem to predict the existence of the 0^+ resonance. Imposing that the phase shift crosses the value $\pi/2$ at the resonance energy improves the situation, though not dramatically. Following a previous suggestion [26], Ref. [27] used not only the available resonance energy, but also the width [24] to constrain these parameters. The obtained values for $a_0 = -1.76\times 10^3$ fm, $r_0 = 1.096$ fm, and $\mathcal{P}_0 = -1.654$ fm^3 made use of the resonance energy and width from Ref. [24]. Later we compare these numbers with the ones from our EFT fits.

At energies below $E_{LAB} = 3$ MeV data were obtained, and a phase-shift analysis performed, by Ref. [28]. Values of the latter can be found in Table II of the review [20]. Since it is well-determined experimentally, and due to its relevance to the triple-alpha process, we use the 0^+ resonance parameters from Ref. [25] as important constraints. This is in line with the EFT approach, where lower-energy observables have preference over higher-energy ones. The relationship among the EFT parameters and the resonance energy and width allows one to reduce the number of variables to be adjusted at each order in the power counting.

Below, we also show the ERE from Ref. [27] for orientation, and comment on the extremely large value of the scattering length a_0, which suggests a large amount of fine-tuning in the parameters of the underlying theory away from the naturalness assumption.

In the power counting that we discussed for the $\alpha\alpha$ system, the amplitude T_{CS} for generic momenta is given up to NLO by Eq. (17). As demonstrated in the previous subsection, this expression combines the deep-non-perturbative Coulomb approximation (14) for the function H with the expansion around the resonance pole, thus preventing the need for multiple kinematical fine-tunings. In LO, the two parameters a_0 and $\tilde{r}_0$ can be obtained from the constraints (18) and (21). At NLO, a fit to scattering data is needed to determine $\tilde{\mathcal{P}}_0$.

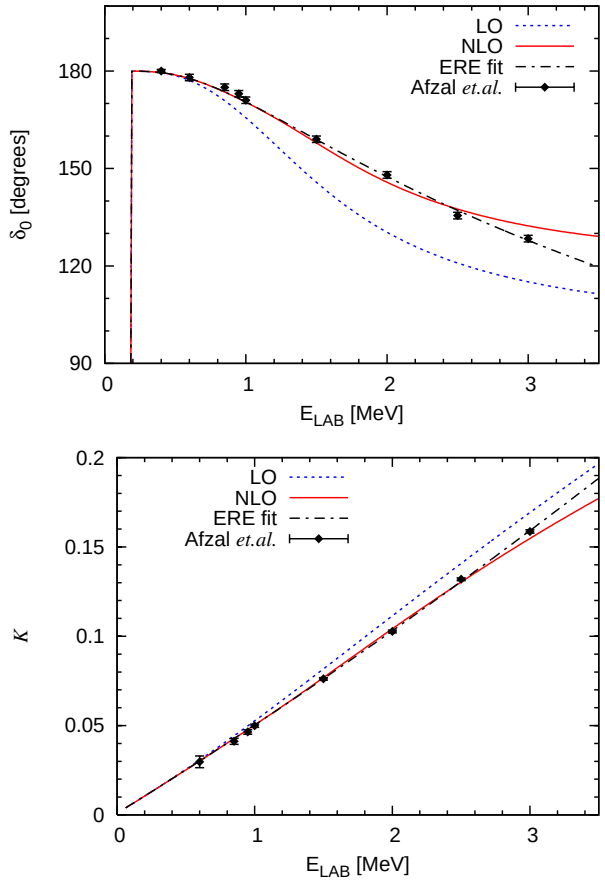

Fig. 2. EFT results for $\alpha\alpha$ scattering at LO (dotted) and NLO (solid), compared against the data. Top panel: phase shift δ_0^c. Bottom panel: $K(\eta) \equiv C_\eta^2(\cot\delta_0^c - i)/2\eta + H(\eta)$.

Figure 2 shows our results with the resonance position and width constraints, compared to the available S-wave phase shifts below $E_{LAB} = 3$ MeV. In the region above the resonance, where scattering data are shown, the LO curve is a prediction, which is consistent with the first few points but then moves away from the data. The NLO curve has $\tilde{\mathcal{P}}_0$ as an extra parameter, which is determined from a global χ^2-fit to scattering data shown. As expected from a convergent expansion, the description of the low-energy data improves with increasing order. At about 3 MeV and above, higher-order contributions are expected to be important, as suggested by the discussion on the relevant scales and manifest in the growing difference between the NLO curve and both LO curve and data points. Also shown are results from a fit using the conventional ERE formula, Eq. (15), in order to stress the differences between this and our EFT approach.

Table 1 shows the values of ERE parameters used to produce the curves of Fig. 2, and compare them with the values [27] obtained from effective range theory. At LO, our values for a_0 and r_0 are consistent with the ones from Ref. [27], remarkably r_0. The NLO corrections, however, spoil this initial LO agreement. The reason for this deviation could be due to the way the width constraint was obtained in Ref. [27]. Its Eq. (4) reads

$$\frac{dh}{dk^2}(\eta_R) - \frac{1}{\mu\Gamma(E_R)}\frac{\pi}{e^{2\pi k_C/k_R}-1} = \frac{1}{4k_C}\left(r_0 - \mathcal{P}_0\, k_R^2\right), \quad (24)$$

where $h(\eta) \equiv \mathrm{Re}[H(\eta)]$. Following this reference's procedure, we reproduced the quoted value of the width (6.4 eV) only when $dh(\eta_R)/dk^2$ was approximated by $1/12k_C^2$ [see Eq. (14)]. However, that is equivalent to neglect the electromagnetic term of $\tilde{\mathcal{P}}_0$ in Eq. (21), which is inconsistent since the strong piece contributes at the same order. Neglecting this term explains the agreement at LO and disagreement at NLO between our and Ref. [27] numbers for r_0. With a smaller r_0, and therefore larger (negative) $\tilde{r}_0$, one can also understand why Ref. [27] obtains a smaller a_0, as the product $\tilde{r}_0 a_0$ is inversely proportional to the resonance momentum squared. By repeating the Ref. [27]'s procedure including the width constraint consistently, we obtained essentially the same values as in our EFT fits. This updated ERE fit is also shown in Table 1.

	a_0 (10^3 fm)	r_0 (fm)	$\mathcal{P}_0$ (fm^3)
LO	-1.80	1.083	—
NLO	-1.92 ± 0.09	1.098 ± 0.005	-1.46 ± 0.08
ERE (our fit)	-1.92 ± 0.09	1.099 ± 0.005	-1.62 ± 0.08
ERE [27]	-1.65 ± 0.17	1.084 ± 0.011	-1.76 ± 0.22

Table 1. ERE parameters extracted from EFT fits in the first two orders, compared with values from two ERE fits, our own and Ref. [27]'s.

Our fits reveal both effective range $r_0 \sim 1/(180\ \mathrm{MeV})$ and shape parameter $\mathcal{P}_0 \sim 1/(170\ \mathrm{MeV})^3$ scaling with powers of M_{hi}, in agreement with our *a priori* estimate. The relative errors in a_0 and $\tilde{r}_0$ at LO are estimated to be of the order of the EFT parameter expansion, $M_{lo}/M_{hi} \sim 1/7 \approx 15\%$. At NLO, the main source of uncertainty comes from the precision of the most recent measurement of the resonance width [25], lying between 4–5%. The uncertainty in $\tilde{\mathcal{P}}_0$, given by the χ^2-fit, is of the same order. Note that the small relative error in r_0 compared to the one in

$\tilde{r}_0$ is due to the former being an order of magnitude larger than the latter, as we discuss in the next subsection. The NLO errors found here are a factor of two smaller than the ones obtained by Ref. [27].

One should stress that the accurate value of the resonance width, $\Gamma_R = 5.57 \pm 0.25$ eV, imposes tight constraints on our fits, through a_0 and r_0. A significant improvement in our NLO fit and overall agreement with data is observed. But looking in detail, one sees that the theoretical curve is not able to cross the error bands of many scattering points below 3 MeV. This can be inferred from the χ^2/datum $\simeq 4$. In principle, a better agreement should be achieved by an N^{2}LO calculation. However, that would introduce an extra parameter that is mostly determined by the scattering data, and an expected agreement could mask any possible inconsistencies between the phase shifts and the resonance parameters. The high NLO χ^2/datum suggests that they are not compatible with each other or, at least, one of them has overestimated precision. As a test we fitted both our NLO EFT and ERE expressions to the scattering data without the constraints from the resonance width. In these two cases, description of S-wave phase shifts is much better at the expense of an underpredicted resonance width, $\Gamma_R = 4.9 \pm 0.6$ eV with ERE and $\Gamma_R = 2.87 \pm 0.23$ eV with EFT. The ERE result is still consistent with the measured Γ_R thanks to its large error bar. In EFT, where lower-energy data have higher priority, the discrepancy is amplified. The problem is even more pronounced if the fit is performed using data up to 2.5 MeV instead of 3 MeV: the results $\Gamma_R = 4.2 \pm 0.6$ eV with ERE and $\Gamma_R = 2.93 \pm 0.34$ eV with EFT fall beyond the quoted experimental error bars. Oddly, this tendency continues as one lowers the upper limit in the fit. Reanalyses of the existing low-energy data or even new measurements seem necessary to resolve this discrepancy.

3.4 fine-tuning puzzle

A surprising feature of the $\alpha\alpha$ system is the very large magnitude of a_0, even if compared to the large scattering length observed in the nucleon-nucleon system. The latter case is thought to be the outcome of a fine-tuning in the QCD parameters, giving rise to an anomalously low momentum scale. It is plausible to expect that this fine-tuning propagates to heavier systems. However, the enormous value of a_0 in the $\alpha\alpha$ is suggestive of a more delicate tuning, with electromagnetic interactions playing a crucial role.

To better understand the puzzle it is worth looking in details at Eq. (11). The Coulomb loop contributions, proportional to the curly brackets, scale as M_{hi}^2/μ, given that $g^2/2\pi \sim M_{hi}/\mu^2$ and $2k_C \sim M_{hi}$. For the scaling $\Delta^{(R)} \sim M_{lo}^2/\mu$ to hold the scale-dependent parameter $\Delta(\kappa)$ must be of the same size of the Coulomb loops, and strongly cancel each other to produce a result $(M_{lo}/M_{hi})^2 \sim 100$ times smaller. This amount of fine-tuning is necessary to obtain a resonance at the right position. Similar cancellation is observed for the P-wave resonance in $n\alpha$ [17]. However, in the present case the fine-tuning is caused by a delicate balance between the strong and electromagnetic forces.

This fine-tuning scenario becomes even more enigmatic by considering the width. The tiny value of $\Gamma_R \approx 6$ eV is intimately related to the resonance momentum, as can be immediately seen in Eq. (21). That is simply an effect of the Coulomb repulsion—the resonance trapped inside the envelope formed by the strong plus Coulomb potential has to tunnel through a larger potential barrier as its energy gets smaller. The probability of tunneling is proportional to the resonance width, from where the smallness of Γ_R follows. Despite the tiny value, the width has an associated scale of $4\pi k_C/\mu\tilde{r}_0$ which is quite large. A natural estimative for this quantity would be $\sim M_{hi}^2/\mu$, implying that $\tilde{r}_0 \sim 1/M_{hi}$. However, from the width constraint one finds $\tilde{r}_0 \sim M_{lo}/M_{hi}^2$, leading to an r_0 that roughly cancels against $1/3k_C$ with a remainder about 10% smaller. From Eq. (18) one sees that the extra fine-tuning in $\tilde{r}_0$ is responsible for an extra increase in the scattering length by a factor of M_{hi}/M_{lo}, becoming effectively $|a_0| \sim M_{hi}^2/M_{lo}^3$. It is remarkable, that if the strong forces generated an r_0 11% larger the ^{8}Be ground state would be bound, with drastic consequences in the formation of elements in the universe (see also Ref.[29]).

4 $p\alpha$ scattering

The $p\alpha$ scattering at low energies is mostly dominated by the $P_{3/2}$ partial wave, due to the presence of a resonance at proton energies $E_p \approx 2$ MeV. S-wave also gives an important contribution for $E_p \leq 5$ MeV, which is the low-energy region we are interested in (see below). In the $P_{1/2}$ wave the phase shift varies smoothly up to $E_p = 18$ MeV, suggesting the existence of a very broad resonance for proton energies between 8 and 15 MeV [30]. However, to the order in the power counting and energies that we consider, it behaves as a typical higher-order effect. Higher wave phase shifts are less than a few fractions of degree below $E_p \approx 6$ MeV, where D-waves start being relevant. Therefore, only two partial waves contribute to the low-energy EFT for the $p\alpha$ system, up to and including NLO.

The Lagrangian for nucleon and alpha particles interacting via $S_{1/2}$ and $P_{3/2}$ partial waves is written as [31,16,17]

$$
\begin{aligned}
\mathcal{L}_{N\alpha} &= \phi^\dagger\left[iD_0 + \frac{\mathbf{D}^2}{2m_\alpha}\right]\phi + N^\dagger\left[iD_0 + \frac{\mathbf{D}^2}{2m_N}\right]N \\
&+\varsigma_{0+}s^\dagger\left[-\Delta_{0+}\right]s + \varsigma_{1+}t^\dagger\left[iD_0 + \frac{\mathbf{D}^2}{2(m_\alpha+m_N)} - \Delta_{1+}\right]t \\
&-\frac{1}{4}F_{\mu\nu}F^{\mu\nu} + \frac{g_{1+}}{2}\left\{t^\dagger\mathbf{S}^\dagger\cdot\left[N\mathbf{D}\phi - (\mathbf{D}N)\phi\right] + \text{H.c.}\right. \\
&\left.-r\left[t^\dagger\mathbf{S}^\dagger\cdot\mathbf{D}(N\phi) + \text{H.c.}\right]\right\} + g_{0+}\left[s^\dagger N\phi + \phi^\dagger N^\dagger s\right] \\
&+\varsigma_{0+}s^\dagger\left[iD_0 + \frac{\mathbf{D}^2}{2(m_\alpha+m_N)}\right]s \\
&+g'_{1+}t^\dagger\left[iD_0 + \frac{\mathbf{D}^2}{2(m_\alpha+m_N)}\right]^2 t\,, \qquad (25)
\end{aligned}
$$

Table 2. $P_{3/2}$ pα resonance parameters from the extended R-matrix analysis of Ref. [32].

k_r (MeV)	k_i (MeV)	E_R (MeV)	$\Gamma_R/2$ (MeV)
51.1	9.0	1.69	0.61

Table 3. $S_{1/2}$ and $P_{3/2}$ pα parameters extracted from the ERE fit of Ref. [33].

a_{0+} (fm)	r_{0+} (fm)	
4.97 ± 0.12	1.295 ± 0.082	
a_{1+} (fm^3)	r_{1+} (fm^{-1})	$\mathcal{P}_{1+}$ (fm)
-44.83 ± 0.51	-0.365 ± 0.013	-2.39 ± 0.15

where ϕ and N are the alpha and nucleon fields with masses m_α and m_N, respectively, and

$$r = (m_\alpha - m_N)/(m_\alpha + m_N)\,. \tag{26}$$

The auxiliary dimeron fields t and s couple to $N\alpha$ in $P_{3/2}$ and $S_{1/2}$ waves, with leading-order coupling constants g_{1+} and g_{0+}, respectively. The S_i's are 2×4 spin-transition matrices between $J = 1/2$ and $J = 3/2$ total angular momentum states. The sign variables ς_{0+}, $\varsigma_{1+} = \pm1$ in front of the kinetic term of the dimeron fields are adjusted to reproduce the signs of the respective effective ranges. The gauge-covariant derivative is defined in the usual way in terms of the photon field A_μ,

$$D_\mu = \partial_\mu + ieZ\,\frac{1+\tau_3}{2}\,A_\mu\,, \tag{27}$$

where Z is the charge of the "particle" whose field the covariant derivative acts on, τ_3 is the z-direction Pauli matrix acting in isospin space, and A_μ is the photon field.

The power counting in essence consists of establishing how the size of the (renormalized) EFT coupling constants depend on the momentum scales present in the system one wishes to describe. The former have a direct relation to observables, namely, the ERE parameters. In the $p\alpha$ system one is interested in describing the scattering region around the $P_{3/2}$ resonance located at $k = k_p \sim M_{lo}$, where

$$k_p = k_r - ik_i \tag{28}$$

is the (complex) resonance momentum in terms of real quantities k_r and k_i. Table 2 lists the resonance parameters extracted from the so-called extended R-matrix analysis used in Ref. [32], which indicates that $k_r \sim M_{lo} \sim 50$ MeV and $k_i \sim M_{lo}^2/M_{hi} \sim 10$ MeV. The suppression of k_i relative to k_r matches with narrow character of the $P_{3/2}$ resonance. As in the $\alpha\alpha$ case [18], M_{hi} is set as the momentum required to excite the α core or the pion mass, both around 140 MeV. Our expansion parameter is of the order of 1/3, allowing us to expect convergent results for proton energies up to 5 MeV.

Table 3 shows the numerical values of the $S_{1/2}$ and $P_{3/2}$ ERE parameters taken from Ref. [33]. As we can notice, while $\mathcal{P}_{1+}/4 \sim r_{0+}/2 \sim 1/M_{hi}$ are in agreement with the natural assumption, the quantities $a_{0+} \sim 1/M_{lo}$, $a_{1+} \sim 1/M_{lo}^3$, and $r_{1+}/2 \sim M_{lo}$ are fine-tuned. To be consistent with these scalings the EFT couplings in Eq. (25) must behave as

$$\Delta_{1+}^{(R)} \sim \frac{M_{lo}^2}{2\mu}\,, \quad \frac{g_{1+}^{(R)\,2}}{3\pi} \sim \frac{1}{\mu^2 M_{lo}}\,, \quad \text{and} \quad \frac{g'_{1+}}{4} \sim \frac{\mu}{M_{lo}M_{hi}} \tag{29}$$

in the $P_{3/2}$ channel, and

$$\Delta_{0+}^{(R)} \sim \frac{M_{hi}M_{lo}}{2\mu} \qquad \text{and} \qquad \frac{g_{0+}^2}{\pi} \sim \frac{M_{hi}}{\mu^2} \tag{30}$$

in $S_{1/2}$, where μ now stands for the $p\alpha$ reduced mass. In the latter case the situation is nearly identical to the proton-proton case [19]: up to NLO the $S_{1/2}$ amplitude reads

$$T_{0+} = -\frac{2\pi}{\mu}\,\frac{C_\eta^2 e^{2i\sigma_0}}{-1/a_{0+} - 2k_C H(\eta)}\left[1 - \frac{r_{0+}k^2/2}{-1/a_{0+} - 2k_C H(\eta)}\right]. \tag{31}$$

For P-wave interactions, Coulomb can be introduced in a straightforward way [31]. The evaluation of Feynman diagrams and the necessary resummation results in

$$T_{1+} = -\frac{2\pi}{\mu}\,\frac{C_\eta^{(1)\,2} e^{2i\sigma_1} k^2 P_{1+}(\theta)}{-1/a_{1+} + r_{1+}k^2/2 - 2k_C H^{(1)}(\eta)} \times\left[1 + \frac{\mathcal{P}_{1+}k^4/4}{-1/a_{1+} + r_{1+}k^2/2 - 2k_C H^{(1)}(\eta)}\right], \tag{32}$$

where

$$C_\eta^{(1)\,2} = (1+\eta^2)C_\eta^2\,, \tag{33}$$

$$H^{(1)}(\eta) = k^2(1+\eta^2)H(\eta)\,, \tag{34}$$

and the variable $k_C = Z_\alpha Z_p \mu\alpha_{em}$ is adapted to the $p\alpha$ case. The $P_{3/2}$ projector is given by

$$P_{1+}(\theta) = 2\cos\theta + \boldsymbol{\sigma}\cdot\hat{\mathbf{n}}\sin\theta\,, \tag{35}$$

where θ is the angle between $\mathbf{k}$ and $\mathbf{k}'$ —the initial and final momenta in the center-of-mass frame, respectively— and $\hat{\mathbf{n}} = \mathbf{k}\times\mathbf{k}'/|\mathbf{k}\times\mathbf{k}'|$ is the unit vector normal to the scattering plane. In this form, the T_{1+} amplitude requires the same kinematical fine-tuning discussed in Sect. 3.2. For pragmatical reasons, we therefore adopt the expansion around the resonance pole in this channel.

4.1 $P_{3/2}$ resonance pole expansion

For practical applications, the more efficient way of expressing the EFT amplitude in the presence of low-energy resonances is to perform the resonance pole expansion. One nice feature is that, at every order in the power-counting, the amplitude maintains its resonant behavior at the expected position with the correct magnitude. It is straightforward to extend the ideas outlined in Sect. 3.2 to the present case, with a resonance pole in the fourth quadrant

of the complex momentum plane [31]. With the pole given by Eq. (28) one rewrites Eq. (32) as

$$T_{1+} = -\frac{2\pi}{\mu}\frac{C_\eta^{(1)\,2} e^{2i\sigma_1} k^2 P_{1+}(\theta)}{\frac{\tilde{r}_{1+}}{2}(k^2-k_p^2) - 2k_C\left[H^{(1)}\left(\frac{k_C}{k}\right) - H^{(1)}\left(\frac{k_C}{k_p}\right)\right]} \times\left\{1 + \frac{\mathcal{P}_{1+}(k^2-k_p^2)^2/4}{\frac{\tilde{r}_{1+}}{2}(k^2-k_p^2) - 2k_C\left[H^{(1)}\left(\frac{k_C}{k}\right) - H^{(1)}\left(\frac{k_C}{k_p}\right)\right]}\right\}, \tag{36}$$

where

$$\tilde{r}_{1+} = -k_r\left\{\underbrace{2L_i}_{\text{LO}} - \underbrace{2ik_i\mathcal{P}_{1+}}_{\text{NLO}}\right\} \tag{37}$$

and L_i, L_r are defined at the pole position from

$$2k_C H^{(1)}(k_C/k_p) = k_r^3 L_r + 2ik_r^2 k_i L_i\,. \tag{38}$$

The factors in front of $L_r, L_i \sim O(1)$ reflect the behavior of the Coulomb function $H^{(1)}(\eta)$ around the resonance. Notice that, as in the $\alpha\alpha$ amplitude, T_{1+} is parametrized only in terms of k_r and k_i at LO, with the extra parameter $\mathcal{P}_{1+}$ appearing at NLO.

The $P_{3/2}$ scattering length and effective range are given by

$$\frac{r_{1+}}{2} = -k_r\left[L_i - \frac{k_r\mathcal{P}_{1+}}{2}\left(1-\frac{k_i^2}{k_r^2}\right)\right] \simeq -k_r\left[\underbrace{L_i}_{\text{LO}} - \underbrace{\frac{k_r\mathcal{P}_{1+}}{2}}_{\text{NLO}}\right], \tag{39}$$

$$\frac{1}{a_{1+}} = -k_r^3\left[L_r + L_i\left(1-\frac{k_i^2}{k_r^2}\right) - \frac{k_r\mathcal{P}_{1+}}{4}\left(1+\frac{k_i^2}{k_r^2}\right)^2\right] \simeq -k_r^3\left[\underbrace{L_r + L_i}_{\text{LO}} - \underbrace{\frac{k_r\mathcal{P}_{1+}}{4}}_{\text{NLO}}\right], \tag{40}$$

and nicely show the scalings $1/a_{1+} \sim M_{lo}^3$ and $r_{1+}/2 \sim M_{lo}$ that were expected from the numbers of Table 3.

4.2 results

In order to test our power-counting assumptions, we fit the expressions for the $S_{1/2}$ and $P_{3/2}$ amplitudes to the corresponding phase shifts and compare the obtained ERE parameters with the ones in the literature. We used the numbers from Table 5 of Ref. [33] in our fit. The results are shown in Table 4. In our fits we have assumed that all the points have the same statistical weight, since error bars were not provided. However, we incorporated the EFT systematic error estimates by imposing that the amplitude cannot be reproduced to a precision better than $(k/2m_\pi)^{n+1}$, where k is the CM momentum of the pα system, m_π our

Table 4. $S_{1/2}$ and $P_{3/2}$ pα ERE parameters extracted in our fits at LO and NLO.

order	a_{0+} (fm)	r_{0+} (fm)
LO	$7.4^{+8.0}_{-2.2}$	—
NLO	$4.81^{+0.05}_{-0.21}$	$1.7^{+1.3}_{-0.8}$

order	a_{1+} (fm^3)	r_{1+} (fm^{-1})	$\mathcal{P}_{1+}$ (fm)
LO	$-58.0^{+11.0}_{-29.0}$	$-0.15^{+0.14}_{-0.09}$	—
NLO	$-44.5^{+1.6}_{-0.1}$	$-0.40^{+0.04}_{-0.10}$	$-2.8^{+1.0}_{-1.8}$

Table 5. $P_{3/2}$ $p\alpha$ resonance parameters extracted from our fits at LO and NLO.

$P_{3/2}$	k_r (MeV)	k_i (MeV)	E_R (MeV)	$\Gamma_R/2$ (MeV)
LO	$50.6^{+1.2}$			

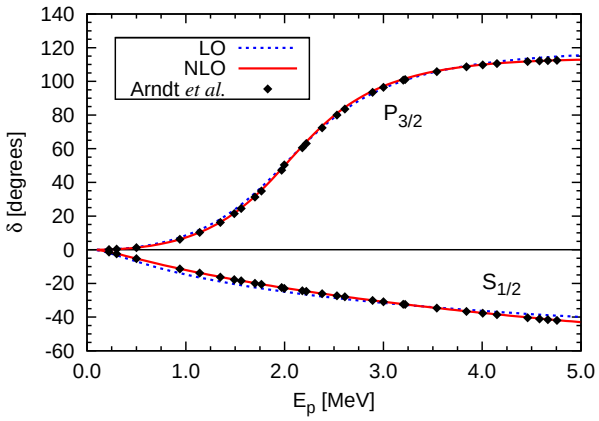

Fig. 3. EFT results for $S_{1/2}$ and $P_{3/2}$ scattering phase shifts at LO (dotted) and NLO (solid), compared against the partial wave analysis results from Arndt *et al.* (diamonds).

measured at the laboratory scattering angle $\theta = 140°$. The sharp enhancement at low energies reflects the characteristic dominance of the Mott cross-section. One clearly sees that already at LO (dotted line) one has a good description of data, especially around the resonance peak. There is a slight improvement at NLO (thick solid line). The curves also agree well with the ERE curve (thin solid line), which uses the ERE formula for the $S_{1/2}$, $P_{3/2}$, and $P_{1/2}$ partial waves and the numerical parameters from Ref. [33]. However, small deviations start to show up at $E_p \approx 3.5$ MeV, indicating an increasing importance of higher order terms as one goes higher in energy. The deviations, which seem to come mainly from the $P_{1/2}$ channel, can be eliminated by going to higher orders in the power counting.

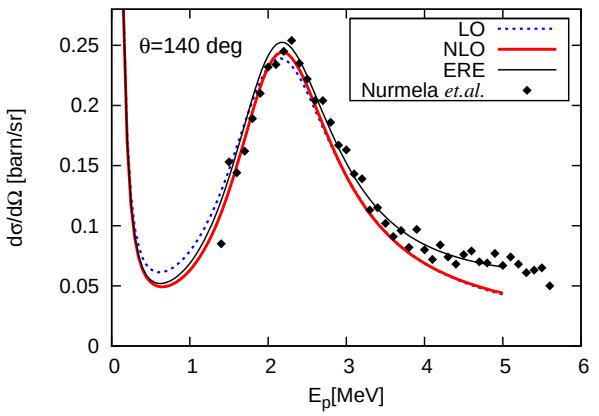

Fig. 4. EFT results at LO (dotted) and NLO (thick solid) for $p\alpha$ elastic cross-section at $\theta = 140°$ laboratory scattering angle, compared against the partial wave analysis results from Arndt *et al.* (thin solid) and measured data point from Ref. [34] (diamonds).

5 summary

I reviewed the programme of halo/cluster EFT suitable to study several interesting nuclear processes that play a role in nuclear astrophysics. I concentrated on two important aspects commonly present in those systems, namely, narrow resonances and Coulomb interactions. The $\alpha\alpha$ and $p\alpha$ interactions were given as examples of how setting up the formalism, then used as practical applications.

The study of the $\alpha\alpha$ interaction revealed a very interesting picture, where the scales of the strong interaction conspire to produce a system with an almost non-relativistic conformal symmetry. One also observed extra amount of fine-tuning once electromagnetic interactions between the particles are turned on, up to the point of generating an S-wave scattering length that is three orders of magnitude larger than the typical range of the interaction. Despite the struggle in understanding the subtle cancellations between the strong and electromagnetic forces, the formalism is quite successful phenomenologically. In fact, thanks to those cancellations we were able to pin down the S-wave effective range parameters with an improved accuracy relative to previous studies.

We extended the formalism to include P-waves with resonance and Coulomb interactions when dealing with the $p\alpha$ system. We performed the expansion of the $P_{3/2}$ amplitude around the resonance pole, which allowed us to extract the resonance properties directly from a fit to the phase shift. We derived expressions for the scattering length and effective range in terms of the resonance parameters, that explains the scalings of the former with the low and high momentum scales M_{lo} and M_{hi} of the theory. Our results at LO and NLO exhibit good convergence at a ratio of about 1/3, and the resonance energy and width are consistent with the ones using the extended R-matrix analysis. Comparison with the differential cross-section at 140° laboratory angle reassures the consistency of the power counting, with $P_{1/2}$ contribution starting to show up only for proton energies beyond 3.5 MeV.

The $\alpha\alpha$ and nucleon-α interactions are the basic ones before considering more complicated clusters of α and nucleons. An interesting example is the Hoyle state in ^{12}C, which plays a key role in the triple-alpha reaction responsible for the formation of heavy elements. A model-study with this state in mind was developed in Ref.[35], where a perturbative treatment of the Coulomb interaction was proposed. This idea might be useful to handle the technical difficulties involving three charged particles.

Acknowledgments

I would like to thank Hans-Werner Hammer, Bira van Kolck, and Carlos Bertulani for stimulating collaboration, and the organizers of the 19th International IUPAP Few-Body Conference 2009 for the opportunity to present this talk. This work was supported by the BMBF under contract number 06BN411.

References

1. H. A. Bethe, Phys. Rev. **76**, 38 (1949).
2. U. van Kolck, Nucl. Phys. **A645**, 273 (1999).
3. J.-W. Chen, G. Rupak, and M.J. Savage, Nucl. Phys. **A653**, 386 (1999); Phys. Lett. **B464**, 1 (1999).
4. G. Rupak, Nucl. Phys. **A678**, 405 (2000).
5. L.H. Thomas, Phys. Rev. **47**, 903 (1935); V. Efimov, Phys. Lett. **33B**, 563 (1970).
6. E. Braaten and H.-W. Hammer, Phys. Rept. **428**, 259 (2006).
7. P.F. Bedaque and U. van Kolck, Ann. Rev. Nucl. Part. Sci. **52**, 339 (2002).
8. P.F. Bedaque, H.-W. Hammer, and U. van Kolck, Nucl. Phys. **A676**, 357 (2000).
9. L. Platter, Phys. Rev. C **74**, 037001 (2006).
10. L. Platter, H.-W. Hammer, and U.-G. Meißner, Phys. Lett. **B607**, 254 (2005).
11. L. Platter, Few Body Syst. **46**, 139 (2009).
12. M. C. Birse, J. A. McGovern, and K. G. Richardson, Phys. Lett. **B464**, 169 (1999).
13. D. L. Canham and H.-W. Hammer, Eur. Phys. J. A **37**, 367 (2008).
14. A.E.A. Amorim, T. Frederico, and L. Tomio, Phys. Rev. C **56**, R2378 (1997); L. Tomio, M.T. Yamashita, and T. Frederico, Mod. Phys. Lett. A **24**, 998 (2009).
15. D. L. Canham and H.-W. Hammer, arXiv:0911.3238v1 [nucl-th].
16. C. A. Bertulani, H.-W. Hammer, and U. van Kolck, Nucl. Phys. **A712**, 37 (2002).
17. P. F. Bedaque, H.-W. Hammer, and U. van Kolck, Phys. Lett. **B569**, 159 (2003).
18. R. Higa, H.-W. Hammer, and U. van Kolck, Nucl. Phys. **A809**, 171 (2008).
19. X. Kong and F. Ravndal, Phys. Lett. **B450** 320 (1999); Nucl. Phys. **A665**, 137 (2000).
20. S.A. Afzal, A.A.Z. Ahmad, and S. Ali, Rev. Mod. Phys. **41**, 247 (1969).
21. T. Mehen, I.W. Stewart, and M.B. Wise, Phys. Lett. **B474**, 145 (2000).
22. D.R. Phillips, G. Rupak, and M.J. Savage, Phys. Lett. **B473**, 209 (2000).
23. B.A. Gelman, Phys. Rev. C **80**, 034005 (2009).
24. J. Benn, E.B. Dally, H.H. Müller, R.E. Pixley, H.H. Staub, and H. Winkler, Nucl. Phys. **A106**, 296 (1967).
25. S. Wüstenbecker, H.W. Becker, H. Ebbing, W.H. Schulte, M. Berheide, M. Buschmann, C. Rolfs, G.E. Mitchell, and J.S. Schweitzer, Z. Phys. A **344**, 205 (1992).
26. T.A. Tombrello, Phys. Lett. **23**, 106 (1966).
27. G. Rasche, Nucl. Phys. **A94**, 301 (1967).
28. N.P. Heydenburg and G.M. Temmer, Phys. Rev. **104**, 123 (1956).
29. H. Oberhummer, A. Csótó, and H. Schlattl, Science **289**, 88 (2000).
30. D.R. Tilley, C.M. Cheves, J.L. Godwin, G.M. Hale, H.M. Hofmann, J.H. Kelley, C.G. Sheu, and H.R. Weller, Nucl. Phys. **A708**, 3 (2002).
31. R. Higa, C.A. Bertulani, and U. van Kolck, in preparation.
32. A. Csótó and G.M. Hale, Phys. Rev. C **55**, 536 (1997).
33. R.A. Arndt, D.L. Long, and L.D. Roper, Nucl. Phys. A **209**, 429 (1973).
34. A. Nurmela, E. Rauhala, and J. Räisänen, J. Appl. Phys. **82**, 1983 (1997).
35. H.-W. Hammer and R. Higa, Eur. Phys. J. A **37**, 193 (2008).